Ligand Bridging-Angle-Driven Assembly of Molecular Architectures Based on Quadruply Bonded Mo−Mo Dimers

Jian-Rong Li,[†] Andrey A. Yakovenko,[†] Weigang Lu,[†] Daren J. Timmons,[‡]
Wenjuan Zhuang,[†] Daqiang Yuan,[†] and Hong-Cai Zhou*,[†]

*Departments of Chemistry, Texas A&M University, P.O. Box 30012, College Station,
Texas 77842-3012, United States, and Virginia Military Institute, Lexington,
Virginia 24450, United States*

Received September 7, 2010; E-mail: zhou@mail.chem.tamu.edu

Abstract: A systematic exploration of the assembly of $Mo_2(O_2C-)_4$-based metal−organic molecular architectures structurally controlled by the bridging angles of rigid organic linkers has been performed. Twelve bridging dicarboxylate ligands were designed to be of different sizes with bridging angles of 0, 60, 90, and 120° while incorporating a variety of nonbridging functional groups, and these ligands were used as linkers. These dicarboxylate linkers assemble with quadruply bonded Mo−Mo clusters acting as nodes to give 13 molecular architectures, termed metal−organic polygons/polyhedra with metal cluster node arrangements of a linear shape, triangle, octahedron, and cuboctahedron/anti-cuboctahedron. The syntheses of these complexes have been optimized and their structures determined by single-crystal X-ray diffraction. The results have shown that the shape and size of the resulting molecular architecture can be controlled by tuning the bridging angle and size of the linker, respectively. Functionalization of the linker can adjust the solubility of the ensuing molecular assembly but has little or no effect on the geometry of the product. Preliminary gas adsorption, spectroscopic, and electrochemical properties of selected members were also studied. The present work is trying to enrich metal-containing supramolecular chemistry through the inclusion of well-characterized quadruply bonded Mo−Mo units into the structures, which can widen the prospect of additional electronic functionality, thereby leading to novel properties.

Introduction

Metal−organic molecular architectures, such as capsules, boxes, polyhedral cages, and polygonal grids/rings, have attracted significant research interest in the past two decades, owing to their fascinating structures and relevance in mechanistic study of self-assembly in nature, as well as intriguing potential for application in materials science and host−guest chemistry-related issues.[1−3] Though difficult, the design and construction of metal-containing supramolecular assemblies with desired structures and functions is becoming more controllable in the chemistry community after long-term exploration of synthetic approaches and the underlying assembly rules involving both inorganic and organic components.[1a,b,d,g,4,5] In some cases, not only the shape and size but also the function of the target assembly can be predesigned, thereby fabricating a particular molecular host for a special application, such as acting as a molecular reactor and a molecular catalytic box.[3b,6,7]

Among metal−organic molecular architectures with various structures, polygonal rings and polyhedral cages are desirable because of their fixed geometric shape and highly cooperative stability.[4f,8] Previously, a variety of highly symmetrical metal−organic polygons and polyhedra have been synthesized by using highly directional organic bridging ligands to bind geometrically pre-fixed metal-containing nodes.[1b,f,h,g,8−15] Most of these reported molecular assemblies were constructed with single metal ions as connecting nodes and neutral organic ligands as linkers.[1b,h,4a,10] The assembly of molecular architectures with multimetal entities or metal clusters acting as nodes has not been widely explored, particularly those of molecular polygons and polyhedra.[1g,11−15] In contrast, multimetal node-based metal−organic frameworks (MOFs) are pervasive, and most reported MOFs contain molecular cages or rings as higher level building units.[16−18] A concentrated study of molecular metal−organic assemblies should result in a greater control in the construction of MOFs, and certain molecular assemblies have

[†] Texas A&M University.
[‡] Virginia Military Institute.
(1) (a) Caulder, D. L.; Raymond, K. N. *Acc. Chem. Res.* **1999**, *32*, 975–982. (b) Leininger, S.; Olenyuk, B.; Stang, P. *Chem. Rev.* **2000**, *100*, 853–908. (c) Dinolfo, P. H.; Hupp, J. T. *Chem. Mater.* **2001**, *13*, 3113–3125. (d) Gianneschi, N. C.; Maser, M. S.; Mirkin, C. A. *Acc. Chem. Res.* **2005**, *38*, 825–837. (e) Pitt, M. A.; Johnson, D. W. *Chem. Soc. Rev.* **2007**, *36*, 1441–1453. (f) Lee, S. J.; Lin, W. *Acc. Chem. Res.* **2008**, *41*, 521–537. (g) Tranchemontagne, D. J.; Ni, Z.; O'Keeffe, M.; Yaghi, O. M. *Angew. Chem., Int. Ed.* **2008**, *47*, 5136–5147. (h) Yoshizawa, M.; Klosterman, J. K.; Fujita, M. *Angew. Chem., Int. Ed.* **2009**, *48*, 3418–3438. (i) Ward, M. D. *Chem. Commun.* **2009**, 4487–4499. (j) Stoddart, J. F. *Nature Chem.* **2009**, *1*, 14–15.

(2) (a) Olenyuk, B.; Whiteford, J. A.; Fechtenkötter, A.; Stang, P. J. *Nature* **1999**, *398*, 796–799. (b) Takeda, N.; Umemoto, K.; Yamaguchi, K.; Fujita, M. *Nature* **1999**, *398*, 794–796. (c) Hong, M.; Zhao, Y.; Su, W.; Cao, R.; Fujita, M.; Zhou, Z.; Chan, A. S. C. *J. Am. Chem. Soc.* **2000**, *122*, 4819–4820. (d) Lee, S. J.; Mulfort, K. L.; Zuo, X.; Goshe, A. J.; Wesson, P. J.; Nguyen, S. T.; Hupp, J. T.; Tiede, D. M. *J. Am. Chem. Soc.* **2008**, *130*, 836–838. (e) Ronson, T. K.; Fisher, J.; Harding, L. P.; Rizkallah, P. J.; Warren, J. E.; Hardie, J. M. *Nature Chem.* **2009**, *1*, 212–216. (f) Beyler, M.; Heitz, V.; Sauvage, J.-P. *J. Am. Chem. Soc.* **2010**, *132*, 4409–4417. (g) Sun, Q.-F.; Iwasa, J.; Ogawa, D.; Ishido, Y.; Sato, S.; Ozeki, T.; Sei, Y.; Yamaguchi, K.; Fujita, M. *Science* **2010**, *328*, 1144–1147.

already been utilized directly as precursors for the preparation of MOFs.[11j,18]

Mining of the inorganic small-molecule library reveals an enormous range of multimetal entities (e.g. multinuclear metal carboxylates) potentially adoptable as nodes for the construction of diverse molecular architectures. An additional advantage of using multimetal nodes comes from the inclusion of their inherent properties, such as stability and magnetism, into the supramolecular systems, resulting in additional interesting properties and functions. These characteristics can widen the spectrum of metal-containing supramolecular chemistry.

Most multimetal node-based molecular polygonal and polyhedral architectures reported contain the paddlewheel $Cu_2(O_2C-)_4$ structural unit, likely because of the ease of preparation; however, these are difficult to study in solution.[11]

In this work, we propose that the use of the quadruply bonded Mo–Mo dinuclear unit $Mo_2(O_2C-)_4$ as a structural base will enable construction of molecular metal–organic assemblies amenable to study in solution by methods such as UV–vis, NMR, and CV. The introduction of metal–metal bonded clusters into molecular assemblies was pioneered by Cotton and Chisholm.[12,13] While other groups also reported a few interesting molecular assembles containing similar metal–metal bonded clusters during that time and thereafter,[14] including our own cuboctahedral and anti-cuboctahedral cages,[15] very few Mo–Mo cluster-containing supramolecular polyhedral cages[13a] have been investigated before this work.

To expand this fascinating chemistry, herein we report a systematic study on the construction of molecular metal–organic architectures with quadruply bonded Mo–Mo dimers and 12 angular dicarboxylate ligands. The quadruply bonded Mo–Mo paddlewheel unit in the form of $Mo_2(O_2CR)_4$ is robust and can be preserved in the molecular assemblies. Four carboxylates surround each paddlewheel to form a square unit. Linkage from

(3) (a) Pluth, M. D.; Bergman, R. G.; Raymond, K. N. *Science* **2007**, *316*, 85–88. (b) Koblenz, T. S.; Wassenaar, J.; Reek, J. N. H. *Chem. Soc. Rev.* **2008**, *37*, 247–262. (c) Jung, M.; Kim, H.; Baek, K.; Kim, K. *Angew. Chem., Int. Ed.* **2008**, *47*, 5755–5757. (d) Sawada, T.; Yoshizawa, M.; Sato, S.; Fujita, M. *Nature Chem.* **2009**, *1*, 53–56. (e) Pluth, M. D.; Bergman, R. G.; Raymond, K. N. *Acc. Chem. Res.* **2009**, *42*, 1650–1659. (f) Duriska, M. B.; Neville, S. M.; Lu, J.; Iremonger, S. S.; Boas, J. F.; Kepert, C. J.; Batten, S. R. *Angew. Chem. Int. Ed.* **2009**, *48*, 8919–8922. (g) Mal, P.; Breiner, B.; Rissanen, K.; Nitschke, J. R. *Science* **2009**, *324*, 1697–1699. (h) Ono, K.; Yoshizawa, M.; Akita, M.; Kato, T.; Tsunobuchi, Y.; Ohkoshi, S.; Fujita, M. *J. Am. Chem. Soc.* **2009**, *131*, 2782–2783. (i) Sato, S.; Morohara, O.; Fujita, D.; Yamaguchi, Y.; Kato, K.; Fujita, M. *J. Am. Chem. Soc.* **2010**, *132*, 3670–3671. (j) Yamauchi, Y.; Hanaoka, Y.; Yoshizawa, M.; Akita, M.; Ichikawa, T.; Yoshio, M.; Kato, T.; Fujita, M. *J. Am. Chem. Soc.* **2010**, *132*, 9555–9557. (k) Hastings, C. J.; Pluth, M. D.; Bergman, R. G.; Raymond, K. N. *J. Am. Chem. Soc.* **2010**, *132*, 6938–6940. (l) Morita, Y.; Yakiyama, Y.; Nakazawa, S.; Murata, T.; Ise, T.; Hashizume, D.; Shiomi, D.; Sato, K.; Kitagawa, M.; Nakasuji, K.; Takui, T. *J. Am. Chem. Soc.* **2010**, *132*, 6944–6946. (m) Flynn, D. C.; Ramakrishna, G.; Yang, H.-B.; Northrop, B. H.; Stang, P. J.; Goodson, T., III *J. Am. Chem. Soc.* **2010**, *132*, 1348–1358.

(4) (a) Fujita, M.; Umemoto, K.; Yoshizawa, M.; Fujita, N.; Kusukawa, T.; Biradha, K. *Chem. Commun.* **2001**, 509–518. (b) Swiegers, G. F.; Malefetse, T. J. *Coord. Chem. Rev.* **2002**, *225*, 91–121. (c) Ercolani, G. *J. Am. Chem. Soc.* **2003**, *125*, 16097–16103. (d) McKinlay, R. M.; Cave, G. W. V.; Atwood, J. L. *Proc. Natl. Acad. Sci. U.S.A.* **2005**, *102*, 5944–5948. (e) Hamilton, T.; Papaefstathiou, G. S.; Friščić, T.; Bučar, D.-K.; MacGillivray, L. R. *J. Am. Chem. Soc.* **2008**, *130*, 14366–14367. (f) Northrop, B. H.; Zheng, Y.-R.; Chi, K.-W.; Stang, P. J. *Acc. Chem. Res.* **2009**, *42*, 1554–1563.

(5) Li, J.-R.; Zhou, H.-C. *Nature Chem.* **2010**, *2*, 893–898.

(6) (a) Murase, T.; Horiuchi, S.; Fujita, M. *J. Am. Chem. Soc.* **2010**, *132*, 2866–2867. (b) Suzuki, K.; Sato, S.; Fujita, M. *Nature Chem.* **2010**, *2*, 25–29.

(7) (a) Lee, S. J.; Cho, S.-H.; Mulfort, K. L.; Tiede, D. M.; Hupp, J. T.; Nguyen, S. T. *J. Am. Chem. Soc.* **2008**, *130*, 16828–16829. (b) Brown, C. J.; Bergman, R. G.; Raymond, K. N. *J. Am. Chem. Soc.* **2009**, *131*, 17530–17531.

(8) (a) Nitschke, J. R.; Lehn, J.-M. *Proc. Natl. Acad. Sci. U.S.A.* **2003**, *100*, 11970–11974. (b) Larsen, R. W. *J. Am. Chem. Soc.* **2008**, *130*, 11246–11247. (c) Sato, S.; Ishido, Y.; Fujita, *J. Am. Chem. Soc.* **2009**, *131*, 6064–6065. (d) Lu, Z.; Knobler, C. B.; Furukawa, H.; Wang, B.; Liu, G.; Yaghi, O. M. *J. Am. Chem. Soc.* **2009**, *131*, 12532–12533. (e) Frischmann, P. D.; Guieu, S.; Tabeshi, R.; MacLachlan, M. J. *J. Am. Chem. Soc.* **2010**, *132*, 7668–7675.

(9) (a) Huang, X.-C.; Zhang, J.-P.; Chen, X.-M. *J. Am. Chem. Soc.* **2004**, *126*, 13218–13219. (b) Sava, D. F.; Kravtsov, V. Ch.; Eckert, J.; Eubank, J. F.; Nouar, F.; Eddaoudi, M. *J. Am. Chem. Soc.* **2009**, *131*, 10394–10396. (c) Rit, A.; Pape, T.; Hahn, F. E. *J. Am. Chem. Soc.* **2010**, *132*, 4572–4573. (d) Birkmann, B.; Fröhlich, R.; Hahn, F. E. *Chem. Eur. J.* **2009**, *15*, 9325–9329. (e) Liu, T.; Liu, Y.; Xuan, W.; Cui, Y. *Angew. Chem., Int. Ed.* **2010**, *49*, 4121–4124.

(10) Some recent examples with single ions as nodes: (a) Cao, M.-L.; Wu, J.-J.; Mo, H.-J.; Ye, B.-H. *J. Am. Chem. Soc.* **2009**, *131*, 3458–3459. (b) Clever, G. H.; Tashiro, S.; Shionoya, M. *Angew. Chem., Int. Ed.* **2009**, *48*, 7010–7012. (c) He, Q.-T.; Li, X.-P.; Liu, Y.; Yu, Z.-Q.; Wang, W.; Su, C.-Y. *Angew. Chem., Int. Ed.* **2009**, *48*, 6156–6159. (d) Wang, M.; Zheng, Y.-R.; Ghosh, K.; Stang, P. J. *J. Am. Chem. Soc.* **2010**, *132*, 6282–6283. (e) Hiraoka, S.; Kiyokawa, M.; Hashida, S.; Shionoya, M. *Angew. Chem., Int. Ed.* **2010**, *49*, 138–143.

(11) (a) Moulton, B.; Lu, J.; Mondal, A.; Zaworotko, M. J. *Chem. Commun.* **2001**, 863–864. (b) Eddaoudi, M.; Kim, J.; Wachter, J. B.; Chae, H. K.; O'Keeffe, M.; Yaghi, O. M. *J. Am. Chem. Soc.* **2001**, *123*, 4368–4369. (c) Abourahma, H.; Coleman, A. W.; Moulton, B.; Rather, B.; Shahgaldian, P.; Zaworotko, M. J. *Chem. Commun.* **2001**, 2380–2381. (d) Ni, Z.; Yasser, A.; Antoun, T.; Yaghi, O. M. *J. Am. Chem. Soc.* **2005**, *127*, 12752–12753. (e) Furukawa, H.; Kim, J.; Ockwig, N. W.; O'Keeffe, M.; Yaghi, O. M. *J. Am. Chem. Soc.* **2008**, *130*, 11650–11661. (f) Wisser, B.; Chamayou, A.-C.; Miller, R.; Scherer, W.; Janiak, C. *CrystEngComm* **2008**, *10*, 461–464. (g) Li, J.-R.; Zhou, H.-C. *Angew. Chem., Int. Ed.* **2009**, *48*, 8465–8468. (h) Prakash, M. J.; Zou, Y.; Hong, S.; Park, M.; Bui, M.-P. N.; Seong, G. H.; Lah, M. S. *Inorg. Chem.* **2009**, *48*, 1281–1283. (i) Tonigold, M.; Hitzbleck, J.; Bahnmüller, S.; Langstein, G.; Volkmer, D. *Dalton Trans.* **2009**, 1363–1371. (j) Li, J.-R.; Timmons, D. J.; Zhou, H.-C. *J. Am. Chem. Soc.* **2009**, *131*, 6368–6369. (k) Prakash, M. J.; Oh, M.; Liu, X.; Han, K. N.; Seong, G. H.; Lah, M. S. *Chem. Commun.* **2010**, *46*, 2049–2051.

(12) (a) Cayton, R. H.; Chisholm, M. H.; Huffman, J. C.; Lobkovsky, E. B. *J. Am. Chem. Soc.* **1991**, *113*, 8709–8724. (b) Cotton, F. A.; Lin, C.; Murillo, C. A. *J. Chem. Soc., Dalton Trans.* **1998**, 3151–3153. (c) Byrnes, M. J.; Chisholm, M. H.; Patmore, N. J. *Inorg. Chem.* **2005**, *44*, 9347–9352.

(13) (a) Cotton, F. A.; Daniels, L. M.; Lin, C.; Murillo, C. A. *Chem. Commun.* **1999**, 841–842. (b) Cotton, F. A.; Daniels, L. M.; Lin, C.; Murillo, C. A. *J. Am. Chem. Soc.* **1999**, *121*, 4538–4539. (c) Cotton, F. A.; Lin, C.; Murillo, C. A. *Inorg. Chem.* **2001**, *40*, 575–577. (d) Cotton, F. A.; Lin, C.; Murillo, C. A. *Inorg. Chem.* **2001**, *40*, 472–477. (e) Cotton, F. A.; Lin, C.; Murillo, C. A. *Inorg. Chem.* **2001**, *40*, 478–484. (f) Cotton, F. A.; Lin, C.; Murillo, C. A. *J. Am. Chem. Soc.* **2001**, *123*, 2670–2671. (g) Cotton, F. A.; Lin, C.; Murillo, C. A. *Acc. Chem. Res.* **2001**, *34*, 759–771.

(14) (a) Whelan, E.; Devereux, M.; McCann, M.; McKee, V. *Chem. Commun.* **1997**, 427–428. (b) Selby, H. D.; Roland, B. K.; Zheng, Z. *Acc. Chem. Res.* **2003**, *36*, 933–944. (c) Sudik, A. C.; Ockwig, N. W.; Millward, A. R.; Côté, A. P.; Yaghi, O. M. *J. Am. Chem. Soc.* **2005**, *127*, 7110–7118. (d) Papadaki, I.; Malliakas, C. D.; Bakas, T.; Trikalitis, P. N. *Inorg. Chem.* **2009**, *48*, 9968–9970.

(15) Ke, Y.; Collins, D. J.; Zhou, H.-C. *Inorg. Chem.* **2005**, *44*, 4154–4156.

(16) Long, J. R. Yaghi, O. M. Eds. Special issue on Metal–Organic Frameworks. *Chem. Soc. Rev.*, **2009**.

(17) (a) Perry, J. J., IV; Perman, J. A.; Zaworotko, M. J. *Chem. Soc. Rev.* **2009**, *38*, 1400–1417. (b) Prakash, M. J.; Lah, M. S. *Chem. Commun.* **2009**, 3326–3341. (c) Zhao, X.; He, H.; Hu, T.; Dai, F.; Sun, D. *Inorg. Chem.* **2009**, *48*, 8057–8059. (d) Yuan, D.; Zhao, D.; Sun, D.; Zhou, H.-C. *Angew. Chem., Int. Ed.* **2010**, *49*, 5357–5361. (e) Yan, Y.; Telepeni, I.; Yang, S.; Lin, X.; Kockelmann, W.; Dailly, A.; Blake, A. J.; Lewis, W.; Walker, G. S.; Allan, D. R.; Barnett, S. A.; Champness, N. R.; Schröder, M. *J. Am. Chem. Soc.* **2010**, *132*, 4092–4094.

(18) (a) Ruben, M.; Ziener, U.; Lehn, J.-M.; Ksenofontov, V.; Gütlich, P.; Vaughan, G. B. M. *Chem. Eur. J.* **2005**, *11*, 94–100. (b) Clegg, J. K.; Iremonger, S. S.; Hayter, M. J.; Southon, P. D.; Macquart, R. B.; Duriska, M. B.; Jensen, P.; Turner, P.; Jolliffe, K. A.; Kepert, C. J.; Meehan, G. V.; Lindoy, L. F. *Angew. Chem., Int. Ed.* **2010**, *49*, 1075–1078.
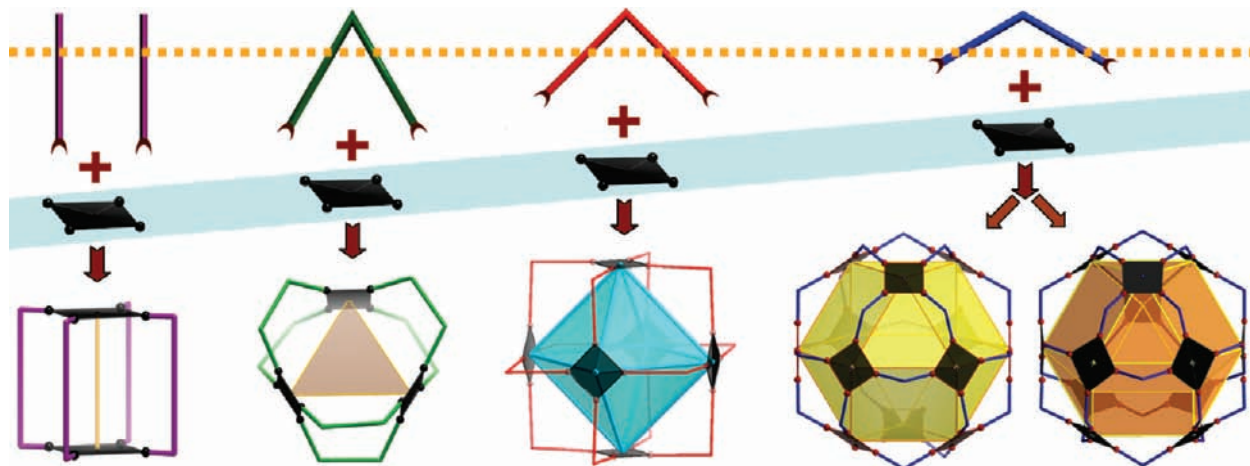
Figure 1. Schematic representation of the assemblies of various angular linkers with a square four-connected node realized in this work.
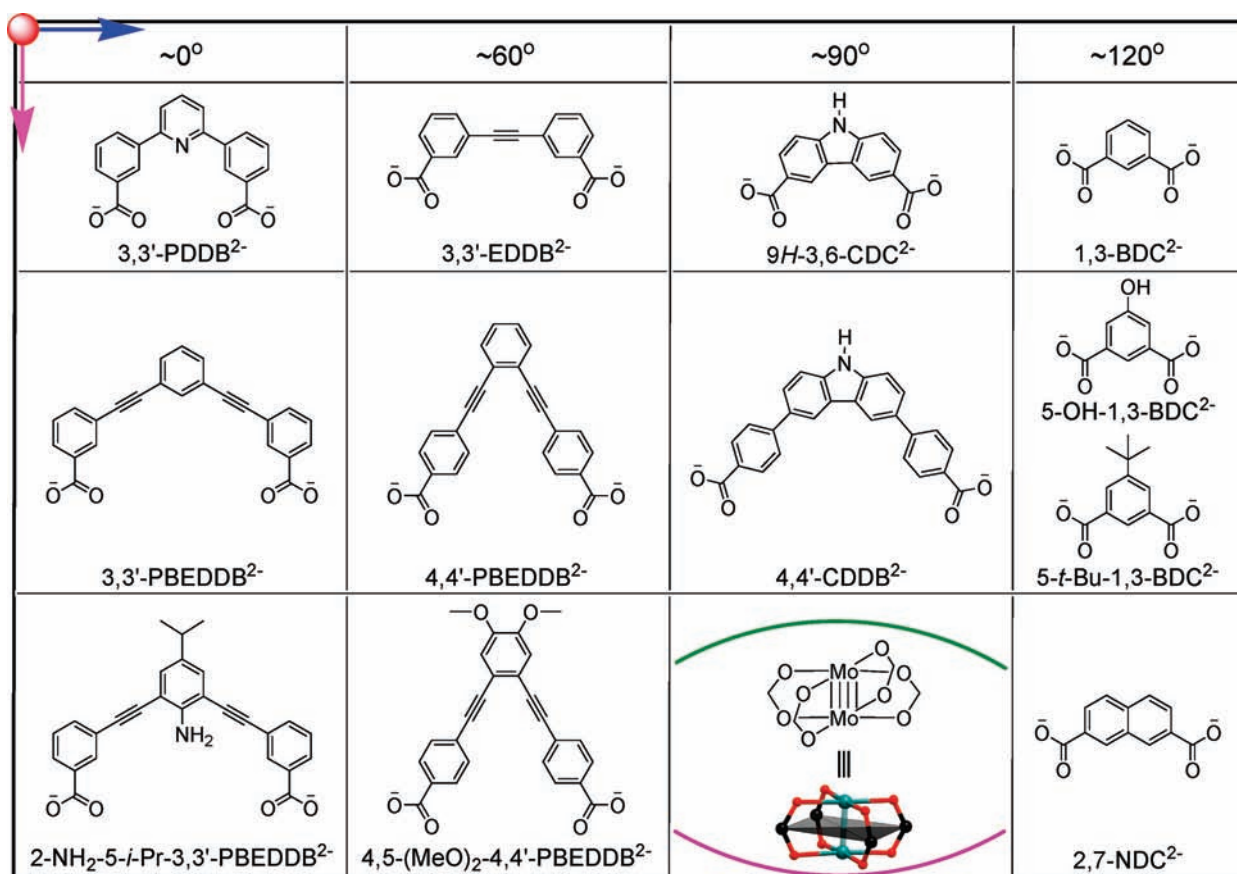

Figure 2. $Mo_2(O_2C-)_4$ cluster and bridging dicarboxylate ligands with different bridging angles, sizes, and nonbridging functional groups used in this work.

the R group can extend the planar square node to a molecular metal−organic architecture. In terms of design principles, in this work the bridging geometry of the organic linker, such as the bend angle of a ditopic bridging ligand, decides the geometrical topology of the resulting molecular architecture, as shown in Figure 1.

Herein, four types of bridging ligands with bridging angles (formed by the two carboxylates in an angular ligand) of 0, 60, 90, and 120° have been designed. It should be pointed out that these four angles are easily attainable in organic synthesis and can be broadly adopted in the construction of other metal−organic architectures with other metal-containing nodes. Thus, as shown

in Figure 2, 12 rigid dicarboxylates (some of them synthesized for the first time) with the four bridging angles and different sizes and nonbridging functional groups have been used to assemble with a Mo−Mo dimer to give 13 corresponding molecular architectures, numbered as **1A**−**4D**. Our study has demonstrated that the geometry of the resulting molecular assembly is dominated by the bridging angle. If the bridging angle is fixed, the size and additional functionalization of the ligand have little effect on the final geometry. Importantly, the nonbridging functional group on the linker plays a critical role in the solubility of the final products, opening a door to the study of solution chemistry. Finally, almost all resulting

molecular assemblies can accommodate axial ligands at both ends of the Mo−Mo units, implying the possibility of extending them into MOF structures.

Experimental Section

Materials and Methods. All the reagents and solvents (AR grade) were commercially available and used as received. Solvents for absorption spectra and CV were further dried in glass contour solvent systems (SG Water USA, LLC) before use. The dicarboxylate ligands were all obtained from their parent diacids during the assembly of the metal−organic architectures. Three parent diacids, i.e., 1,3-benzenedicarboxylic acid [H_2(1,3-BDC)], 5-hydroxy-1,3-benzenedicarboxylic acid [H_2(5-OH-1,3-BDC)], and 5-*tert*-butyl-1,3-benzenedicarboxylic acid [H_2(5-*t*-Bu-1,3-BDC)], were purchased from VWR. One parent diacid, 2,7-naphthalenedicarboxylic acid [H_2(2,7-NDC)], was obtained by the hydrolysis of dimethyl 2,7-naphthalenedicarboxylate, which was purchased from TCI America. Four parent diacids, namely 9*H*-3,6-carbazoledicarboxylic acid [H_2(9*H*-3,6-CDC)],[11j] 3,3′-(2-amino-5-isopropyl-1,3-phenylene)bis(ethyne-2,1-diyl)dibenzoic acid [H_2(2-NH₂-5-*i*-Pr-3,3′-PBEDDB)],[5] and 3,3′-(ethyne-1,2-diyl)dibenzoic acid [H_2(3,3′-EDDB)],[5] were synthesized according to our published procedures. In addition, one parent diacid, 3,3′-[1,3-phenylenebis(ethyne-2,1-diyl)]dibenzoic acid [H_2(3,3′-PBEDDB)], was synthesized by a procedure very similar to that reported during the preparation of this manuscript.[11k] $Mo_2(OAc)_4$[19] and $Mo_2(O_2CCF_3)_4$[20] were prepared by following literature methods. Elemental analyses were performed by Atlantic Microlab, Inc. (Norcross, GA). ¹H NMR data were collected on a Mercury 300 spectrometer. FT-IR data were recorded on an IRAffinity-1 instrument under N_2 atmosphere. The powder X-ray diffraction (PXRD) patterns were recorded on a Bruker D8-Focus Bragg−Brentano X-ray powder diffractometer equipped with a Cu sealed tube ($\lambda = 1.54178$) at room temperature. Crystalline samples were sealed under N_2 atmosphere by a Mylar film for the measurement. Simulation of the PXRD pattern was carried out by using the single-crystal data (after being "squeezed") and diffraction-crystal module of the Mercury program available free of charge via the Internet at http://www.iucr.org. Absorption spectra were recorded on a UV-2450 (Shimadzu) UV/vis spectrophotometer. Electrochemical measurements were made with a model 610A electrochemical analyzer (CH Instrument Inc., USA) using a Pt working electrode, 0.1 M (Bu_4N)(PF_6) supporting electrolyte, and a Ag/AgCl reference electrode. Gas adsorption measurements were performed using an ASAP 2020 volumetric adsorption analyzer.

Synthesis of 3,3′-(Pyridine-2,6-diyl)dibenzoic Acid, [H_2(3,3′-PDDB)]. (a). Dimethyl 3,3′-(Pyridine-2,6-diyl)dibenzoate. 2,6-Dibromopyridine (3.00 g, 12.45 mmol), 3-methoxycarbonylphenylboronic acid (5.40 g, 30.00 mmol), CsF (5.60 g), and Pd(PPh₃)₄ (600 mg) were added to a 250 mL Schlenk flask. The flask was connected to a Schlenk line, evacuated, and refilled with nitrogen gas. Next, 150 mL of 1,2-dimethoxyethane (DME) was degassed and added through a canula. The flask was equipped with a water condenser, and the reaction mixture refluxed under a nitrogen atmosphere for 4 days. The solvent was evaporated on a rotary evaporator. The solid was dissolved in CHCl₃ and washed with water three times. The CHCl₃ solution was dried with sodium sulfate. After CHCl₃ removal, the crude product was washed with 30 mL of acetone to obtain a pure product with ∼60% yield (2.60 g, 7.47 mmol) based on 2,6-dibromopyridine. ¹H NMR (300 MHz, DMSO-d_6): δ 3.98 (s, 6H), 7.59 (t, 2H), 7.79 (d, 2H), 7.88 (t, 1H), 8.11 (d, 2H), 8.45 (d, 2H), 8.73 (s, 2H).

(b). 3,3′-(Pyridine-2,6-diyl)dibenzoic Acid. Dimethyl 3,3′-(pyridine-2,6-diyl)dibenzoate (2.60 g) was dissolved in 60 mL of a mixed solvent of THF and MeOH (v/v = 1:1), to which 25 mL of 2 N NaOH aqueous solution was added. The mixture was stirred

at 50 °C overnight. The organic phase was removed. The aqueous phase was acidified with diluted hydrochloric acid to give a light-gray precipitate, which was filtered and washed with water. Yield: 2.20 g, ∼92%. ¹H NMR (300 MHz, DMSO-d_6): δ 7.69 (t, 2H), 8.03−8.06 (m, 5H), 8.45 (d, 2H), 8.74 (s, 2H). Anal. Calcd for $C_{19}H_{13}NO_4$ (FW = 319.3): C, 71.47; H, 4.10; N, 4.39. Found: C, 71.13; H, 4.12; N, 4.50. FT-IR (neat, cm⁻¹): 2830(w), 2548(w), 1685(s), 1607(w), 1568(m), 1437(s), 1421(w), 1376(w), 1312(m), 1259(s), 1175(w), 1136(w), 1084(w), 988(w), 942(m), 908(m), 805(m), 782(w), 750(s), 696(w), 676(s), 660(w).

Synthesis of 4,4′-(1,2-Phenylenebis(ethyne-2,1-diyl)dibenzoic Acid, [H_2(4,4′-PBEDDB)]. (a). Diethyl 4,4′-(1,2-Phenylenebis(ethyne-2,1-diyl))dibenzoate. Under a nitrogen atmosphere, ethyl 4-bromobenzoate (3.8 mL, 23.8 mmol) was added to a solution of 1,2-diethynylbenzene[21] (1.00 g, 7.9 mmol) in deoxygenated distilled triethylamine (TEA, 40 mL) with Pd(PPh₃)₄ (350 mg, 0.30 mmol) and CuI (25.0 mg, 0.13 mmol) in a 100 mL Schlenk flask at room temperature. After the mixture was stirred at reflux temperature for 24 h, the reaction system was cooled to room temperature, and then a saturated aqueous solution of ammonium chloride and dichloromethane were added. The organic layer was separated, and the aqueous layer was further extracted two times with dichloromethane. The combined dichloromethane layer was washed with brine and dried over sodium sulfate. After evaporation of the dichloromethane, the crude residue was purified by column chromatography on silica gel with dichloromethane/hexane (50%) as eluent to give pure diethyl 4,4′-(1,2-phenylenebis(ethyne-2,1-diyl))dibenzoate as a white solid (2.33 g, 5.53 mmol, 70% yield based on 1,2-diethynylbenzene). ¹H NMR (300 MHz, CDCl₃): δ 1.40 (t, 6H), 4.37 (q, 4H), 7.34 (q, 2H), 7.57 (q, 2H), 7.59 (d, 4H), 8.03 (d, 4H).

(b). 4,4′-(1,2-Phenylenebis(ethyne-2,1-diyl))dibenzoic Acid. Diethyl 4,4′-(1,2-phenylenebis(ethyne-2,1-diyl))dibenzoate (2.33 g) was dissolved in 50 mL of mixed solvent of THF and MeOH (v/v = 1:1), to which 15 mL of 3 N NaOH aqueous solution was added. After the mixture was stirred at about 60 °C overnight, the organic phase was removed. The aqueous phase was filtered and acidified with diluted hydrochloric acid to give a white precipitate, which was filtered and washed with water. Yield: 1.82 g, 90%. ¹H NMR (300 MHz, DMSO-d_6): δ 7.52 (q, 2H), 7.68 (d, 4H), 7.71 (q, 2H), 8.00 (d, 4H). Anal. Calcd for $C_{24}H_{14}O_4$ (FW = 366.4): C, 78.68; H, 3.85. Found: C, 78.42; H, 3.92. FT-IR (neat, cm⁻¹): 2842(w), 2668(w), 2547(w), 2213(w), 1681(s), 1605(s), 1560(m), 1507(w), 1427(m), 1405(w), 1315(s), 1297(s), 1284(s), 1179(m), 1145(w), 1125(w), 1111(w), 948(m), 854(s), 791(w), 759(s), 720(w), 692(s).

Synthesis of 4,4′-(4,5-Dimethoxy-1,2-phenylene)bis(ethyne-2,1-diyl)dibenzoic Acid, [H_2(4,5-(MeO)₂-4,4′-PBEDDB)]. This parent acid was synthesized by following a procedure similar to that for H_2(4,4′-PBEDDB) with only a different starting material of 1,2-dibromo-4,5-dimethoxybenzene instead of 1,2-diiodobenzene. The details are provided in the Supporting Information. ¹H NMR (300 MHz, DMSO-d_6): δ 3.86 (s, 6H), 7.24 (s, 2H), 7.65 (d, 4H), 7.99 (d, 4H). Anal. Calcd for $C_{26}H_{18}O_6$ (FW = 426.4): C, 73.23; H, 4.25. Found: C, 72.96; H, 4.20. FT-IR (neat, cm⁻¹): 2918(w), 2715(w), 2334(w), 1678(s), 1595(m), 1502(m), 1423(m), 1368(w), 1315(s), 1280(s), 1244(s), 1218(s), 1173(m), 1126(w), 1109(w), 1083(m), 999(m), 941(w), 850(s), 793(w), 768(s), 692(s), 642(m).

Synthesis of 4,4′-(9*H*-Carbazole-3,6-diyl)dibenzoic Acid, [H_2(4,4′-CDDB)]. (a). Dimethyl 4,4′-(9*H*-Carbazole-3,6-diyl)dibenzoate. To a 500 mL Schlenk flask were added 3,6-dibromo-9*H*-carbazole[22] (2.00 g, 6.2 mmol), 4-methoxycarbonylphenylboronic acid (3.32 g, 18.5 mmol), CsF (3.45 g), and Pd(PPh₃)₄ (350 mg). The loaded flask was connected to a Schlenk line, evacuated, and refilled with nitrogen gas. DME (200 mL) was degassed and added through a

(19) Brignole, A. B.; Cotton, F. A. *Inorg. Synth.* **1972**, *13*, 81–89.
(20) Cotton, F. A.; Norman, J. G., Jr. *J. Coord. Chem.* **1972**, *1*, 161–171.

(21) Grissom, J. W.; Gunawardena, G. U. *Tetrahedron Lett.* **1995**, *36*, 4951–4954.
(22) Smith, K.; James, D. M.; Mistry, A. G.; Bye, M. R.; Faulkner, D. J. *Tetrahedron* **1992**, *48*, 7479–7488.

canula. The flask was equipped with a water condenser and refluxed under a nitrogen atmosphere for 7 days. The solvent was evaporated on a rotary evaporator. The solid residue was dissolved in a large amount of CHCl$_3$, and the solution was washed with water three times. After the CHCl$_3$ solvent was removed, the crude product was washed with ethyl acetate/hexane (40%) mixed solvent (20 mL) twice and then acetone (30 mL) twice to obtain pure product with ∼55% yield (1.48 g, 3.41 mmol) based on 3,6-dibromo-9H-carbazole. ^{1}H NMR (300 MHz, DMSO-d_6): δ 3.89 (s, 6H), 7.62 (d, 2H), 7.84 (d, 2H), 7.98 (d, 4H), 8.07 (d, 4H), 8.75 (s, 2H), 11.57 (s, 1H).

(b). 4,4′-(9H-Carbazole-3,6-diyl)dibenzoic Acid. Dimethyl 4,4′-(9H-carbazole-3,6-diyl)dibenzoate (1.48 g) was dissolved in 80 mL of mixed solvent of THF and MeOH (v/v = 1:1), to which 20 mL of 2 N NaOH aqueous solution was added. The mixture was stirred at reflux temperature for 24 h. The organic phase was removed. The aqueous phase was acidified with dilute hydrochloric acid to give a gray precipitate, which was filtered and washed with water. Yield: 1.30 g, ∼93%. ^{1}H NMR (300 MHz, DMSO-d_6): δ 7.61 (d, 2H), 7.83 (d, 2H), 7.94 (d, 4H), 8.05 (d, 4H), 8.73 (s, 2H), 11.54 (s, 1H). Anal. Calcd for C$_{26}$H$_{17}$NO$_4$ (FW = 407.4): C, 76.65; H, 4.21; N, 3.44. Found: C, 73.44; H, 4.21; N, 3.67. FT-IR (neat, cm^{-1}): 2946(w), 2669(w), 2551(w), 1676(s), 1605(s), 1560(w), 1518(w), 1488(w), 1424(m), 1316(s), 1268(m), 1234(m), 1187(m), 1131(m), 1109(w), 1081(w), 1007(w), 931(m), 900(w), 877(w), 856(m), 813(m), 769(s), 730(w), 704(m).

Synthesis of Compounds 1A−4D. Compounds **1A−4D** were synthesized similarly using a solvothermal reaction in a sealed glass tube. The detailed synthetic procedure is described only for **1A**. Solvents are abbreviated as follows: DMF, N,N-dimethylformamide; DEF, N,N-diethylformamide; DMA, N,N-dimethylacetamide; NMP, N-methylpyrrolidone; DMSO, dimethyl sulfoxide; and DMPU, 1,3-dimethyl-3,4,5,6-tetrahydro-2(^{1}H)-pyrimidinone.

[Mo$_2$(3,3′-PDDB)$_2$(S)]$_2$, 1A. A 1:2 molar ratio mixture of Mo$_2$(O$_2$CCF$_3$)$_4$ (16 mg, 0.025 mmol) and H$_2$(3,3′-PDDB) (16 mg, 0.050 mmol) was added to a glass tube, to which 1 drop of HBF$_4$ (40% in water) and 1.7 mL of NMP were added successively. The mixture was degassed by two freeze−pump−thaw cycles. The tube was then frozen again in liquid nitrogen and sealed under vacuum. Once the temperature reached room temperature, the sealed mixture was sonicated to allow all solids to dissolve. The tube was heated in a furnace at 85 °C for 2 days and cooled to room temperature spontaneously. In an N$_2$-filled glovebox, single crystals were collected by filtration, washed with 2 × 3 mL of NMP, and then quickly dried on a piece of filter paper to afford 15 mg of crystalline product of [Mo$_2$(3,3′-PDDB)$_2$(S)]$_2$ (**1A**, where **S** represents non-assignable solvent molecules, which are difficult to determine from single-crystal diffraction data due to crystallographic disorder). FT-IR (neat, cm^{-1}): 3432(w), 2933(w), 2873(w), 1653(s), 1570(w), 1538(w), 1507(m), 1475(w), 1457(m), 1438(w), 1405(s), 1374(s), 1301(m), 1267(m), 1178(w), 1159(m), 1111(m), 1047(m), 987(m), 934(m), 870(w), 807(m), 752(s), 735(s), 673(m). This product is unstable in air and insoluble in water, MeOH, EtOH, DMF, DEF, and DMSO. The PXRD pattern of as-synthesized **1A** is shown in Figure S1 (Supporting Information).

[Mo$_2$(3,3′-PBEDDB)$_2$(NMP)$_2$]$_2$, 1B. Following the same procedure as that for **1A** but without the addition of HBF$_4$, a 1:2 molar ratio of Mo$_2$(O$_2$CCF$_3$)$_4$ (16 mg, 0.025 mmol) and H$_2$(3,3′-PBEDDB) (18 mg, 0.050 mmol) reacted in 1.7 mL of NMP at 85 °C for 3 days. Single crystals were collected, washed with NMP, and quickly dried to afford 13 mg of [Mo$_2$(3,3′-PBEDDB)$_2$(NMP)$_2$]$_2$ (**1B**). FT-IR (neat, cm^{-1}): 3455(w), 2900(w), 1653(s), 1560(w), 1541(w), 1506(m), 1472(w), 1456(m), 1423(m), 1404(m), 1385(s), 1298(m), 1261(m), 1171(w), 1112(m), 1082(w), 984(m), 963(w), 907(w), 884(w), 851(w), 815(w), 801(s), 792(s), 754(s), 702(m), 679(m), 665(m). This product is unstable in air and insoluble in water, MeOH, EtOH, DMF, DEF, and DMSO. The PXRD pattern of as-synthesized **1B** is shown in Figure S2 (Supporting Information).

[Mo$_2$(2-NH$_2$-5-i-Pr-3,3′-PBEDDB)$_2$(DMSO)$_2$]$_2$·(DMSO)$_4$, 1C. Following the same procedure as that for **1A** but without the addition of HBF$_4$, a 1:2 molar ratio of Mo$_2$(O$_2$CCF$_3$)$_4$ (16 mg, 0.025 mmol) and H$_2$(2-NH$_2$-5-i-Pr-3,3′-PBEDDB) (21 mg, 0.050 mmol) reacted in 1.5 mL of DMSO at 60 °C for 1 day. Single crystals were collected, washed with DMSO, and quickly dried to afford 16 mg of [Mo$_2$(2-NH$_2$-5-i-Pr-3,3′-PBEDDB)$_2$(DMSO)$_2$]$_2$·(DMSO)$_4$ (**1C**). FT-IR (neat, cm^{-1}): 2938(w), 2202(w), 1685(s), 1605(w), 1558(w), 1538(w), 1507(m), 1472(w), 1438(w), 1424(m), 1387(s), 1302(m), 1236(s), 1130(w), 1014(s), 948(s), 881(w), 854(w), 815(w), 801(s), 757(s), 702(m), 686(m), 655(w). This product is unstable in air and insoluble in water, MeOH, and EtOH but slightly soluble in DMF, DEF, and DMSO. The PXRD pattern of as-synthesized **1C** is shown in Figure S3 (Supporting Information).

[Mo$_2$(3,3′-EDDB)$_2$(S)$_2$]$_3$·xS, 2A. Following the same procedure as that for **1A**, a 1:2 molar ratio of Mo$_2$(O$_2$CCF$_3$)$_4$ (16 mg, 0.025 mmol) and H$_2$(3,3′-EDDB) (13 mg, 0.050 mmol) reacted in 1.7 mL of DMA with 1 drop of HBF$_4$ (40% in water) at 85 °C for 1 day. Single crystals were collected, washed with DMA, and quickly dried to afford 15 mg of [Mo$_2$(3,3′-EDDB)$_2$(S)$_2$]$_3$·xS (**2A**). FT-IR (neat, cm^{-1}): 3440(w), 2931(w), 1701(w), 1617(s), 1560(w), 1539(w), 1509(m), 1457(w), 1414(m), 1386(s), 1263(m), 1190(m), 1080(w), 1059(w), 1015(m), 964(w), 908(w), 814(m), 756(m), 745(s), 683(m), 658(w). This product is unstable in air and insoluble in water, MeOH, EtOH, DMF, DEF, and DMSO. The PXRD pattern of as-synthesized **2A** is shown in Figure S4 (Supporting Information).

[Mo$_6$(4,4′-PBEDDB)$_6$(DMA)$_5$(S)]·xS, 2B, and [Mo$_2$(4,4′-PBEDDB)$_2$(S)$_2$]$_3$·xS, 2B′. Following the same procedure as that for **1A**, a 1:2 molar ratio of Mo$_2$(O$_2$CCF$_3$)$_4$ (16 mg, 0.025 mmol) and H$_2$(4,4′-PBEDDB) (18 mg, 0.050 mmol) reacted in 1.5 mL of DMA with 1 drop of HBF$_4$ (40% in water) at 100 °C for 3 days. In an N$_2$-filled glovebox, the tube was opened, and 1.0 mL of MeOH was carefully layered on the solution. The tube was covered and stood at room temperature for an additional 10 days until needle crystals (**2B**) appeared. Together with the needle crystals, several cubic crystals (**2B′**) also were found to adhere on the wall of tube. Both types of crystals were structurally determined by X-ray diffraction, showing the crystallizations in different space groups. In a glovebox, the solution containing needle single crystals was transferred to a filter, and the crystals were collected by filtration, washed with 1:1 DMA/MeOH, and then quickly dried to afford 10 mg of [Mo$_6$(4,4′-PBEDDB)$_6$(DMA)$_5$(S)]·xS (**2B**). A few cubic crystals of [Mo$_2$(4,4′-PBEDDB)$_2$(S)$_2$]$_3$·xS (**2B′**) attached to the tube wall. Attempts to synthesize pure **2B′** crystals were unsuccessful. Owing to the very low yield of **2B′** in the above synthesis, we did not attempt to collect more samples for other characterizations. FT-IR (neat, cm^{-1}) for **2B**: 3458(w), 2930(w), 1700(w), 1624(s), 1559(w), 1502(m), 1455(w), 1400(s), 1361(w), 1264(m), 1187(m), 1058(w), 1013(m), 962(w), 861(w), 770(m), 740(m), 686(w). Compound **2B** is unstable in air and insoluble in water, MeOH, and EtOH but slightly soluble in DMF, DEF, and DMSO. The PXRD pattern of as-synthesized **2B** is shown in Figure S5 (Supporting Information).

[Mo$_2$(4,5-(MeO)$_2$-4,4′-PBEDDB)$_2$(S)$_2$]$_3$·xS, 2C. Following the same procedure as that for **1A**, a 1:2 molar ratio of Mo$_2$(O$_2$CCF$_3$)$_4$ (16 mg, 0.025 mmol) and H$_2$(4,5-(MeO)$_2$-4,4′-PBEDDB) (21 mg, 0.050 mmol) reacted in 1.8 mL of DMA with 1 drop of HBF$_4$ (40% in water) at 85 °C for 2 days. In an N$_2$-filled glovebox, the tube was opened, and 1.0 mL of MeOH was carefully layered on the solution. The tube was covered and stood at room temperature for 10 additional days to give single crystals of [Mo$_2$(4,5-(MeO)$_2$-4,4′-PBEDDB)$_2$(S)$_2$]$_3$·xS (**2C**), which were collected, washed with 1:1 DMA/MeOH, and quickly dried to afford 8 mg of product. FT-IR (neat, cm^{-1}): 3391(w), 2889(w), 1675(w), 1619(s), 1542(w), 1487(m), 1456(w), 1398(s), 1259(m), 1190(s), 1047(m), 1004(m), 970(w), 848(w), 769(m), 695(m), 653(w). Compound **2C** is unstable in air and insoluble in water, MeOH, and EtOH but slightly soluble

Table 1. Crystal Data and Structure Refinement of **1A**−**1C**

	1A	1B	1C
formula	$C_{38}H_{22}Mo_2N_2O_9$	$C_{116}H_{84}Mo_4N_4O_{20}$	$C_{124}H_{124}Mo_4N_4O_{24}S_8$
formula weight	842.46	2237.63	2694.51
crystal system	tetragonal	triclinic	monoclinic
space group	$I4/m$	$P\bar{1}$	$C2/c$
crystal size, mm	$0.18 \times 0.10 \times 0.10$	$0.28 \times 0.18 \times 0.16$	$0.28 \times 0.20 \times 0.20$
a, Å	12.3235(7)	13.914(4)	21.868(16)
b, Å	12.3235(7)	14.263(4)	30.763(16)
c, Å	24.440(4)	17.484(5)	21.215(13)
α, deg	90	72.778(3)	90
β, deg	90	87.742(3)	90.322(11)
γ, deg	90	67.930(3)	90
V, Å^3	3711.7(7)	3061.3(15)	14271(16)
Z	4	1	4
d_{calc}, g cm^{-3}	1.508	1.214	1.254
reflections collected	9237	30 310	71 880
(before SQUEEZE)	(9568)	(34 844)	(72 985)
independent reflections	1866 [R_{int} = 0.0857]	11 907 [R_{int} = 0.0546]	13 969 [R_{int} = 0.0970]
(before SQUEEZE)	(1966 [R_{int} = 0.0918])	(14 373 [R_{int} = 0.0627])	(14 423 [R_{int} = 0.1080])
data/restraints/parameters	1866/42/77	11 907/28/640	13 969/11/733
(before SQUEEZE)	(1966/42/77)	(14 373/28/641)	(14 423/14/733)
GOF	1.007	1.016	1.015
R_1, $wR_2{}^a$	0.0936, 0.2086	0.0490, 0.1249	0.0671, 0.1632
(before SQUEEZE)	(0.1224, 0.3646)	(0.0906, 0.3413)	(0.1510, 0.4485)

^{a} The value of R_1 is based on "observed" data with $I > 2\sigma(I)$; the value of wR_2 is based on all data.

Table 2. Crystal Data and Structure Refinement of **2A**−**2C**

	2A	2B	2B′	2C
formula	$C_{96}H_{48}Mo_6O_{30}$	$C_{164}H_{117}Mo_6N_5O_{30}$	$C_{144}H_{72}Mo_6O_{30}$	$C_{156}H_{96}Mo_6O_{42}$
formula weight	2256.98	3213.27	2857.66	3217.97
crystal system	monoclinic	monoclinic	cubic	hexagonal
space group	$P2_1/c$	$P2_1/c$	$P\bar{4}3n$	$P6_3/m$
crystal size, mm	$0.28 \times 0.20 \times 0.20$	$0.20 \times 0.10 \times 0.10$	$0.10 \times 0.10 \times 0.10$	$0.20 \times 0.18 \times 0.18$
a, Å	11.620(7)	16.956(5)	35.614(4)	25.807(2)
b, Å	26.165(16)	42.663(12)	35.614(4)	25.807(2)
c, Å	52.45(3)	33.176(8)	35.614(4)	29.780(5)
α, deg	90	90	90	90
β, deg	93.314(8)	113.312(12)	90	90
γ, deg	90	90	90	120
V, Å^3	15 918(17)	22 040(10)	45 170(8)	17 176(4)
Z	4	4	8	2
d_{calc}, g cm^{-3}	0.942	0.968	0.840	0.622
reflections collected	143 102	173 509	11 424	151 822
(before SQUEEZE)	(155 403)	(180 099)	(114 010)	(155 965)
independent reflections	31 156 [R_{int} = 0.0942]	38 754 [R_{int} = 0.1311]	13 269 [R_{int} = 0.2485]	10 274 [R_{int} = 0.2653]
(before SQUEEZE)	(34 935 [R_{int} = 0.1100])	(41 139 [R_{int} = 0.1633])	(14 769 [R_{int} = 0.4944])	(10 713 [R_{int} = 0.5480])
data/restraints/parameters	31 156/6/1159	38 754/76/1060	13 269/68/175	10 274/22/199
(before SQUEEZE)	(34 935/2/1189)	(41 139/76/1090)	(14 769/68/193)	(10 713/22/241)
GOF	1.045	1.013	1.050	1.020
R_1, $wR_2{}^a$	0.0998, 0.2210	0.0912, 0.2029	0.1061, 0.2097	0.0975, 0.1997
(before SQUEEZE)	(0.1914, 0.4745)	(0.1499, 0.4255)	(0.1742, 0.4323)	(0.2025, 0.5566)

^{a} The value of R_1 is based on "observed" data with $I > 2\sigma(I)$; the value of wR_2 is based on all data.

in DMA, DEF, and DMSO. The PXRD pattern of as-synthesized **2C** is shown in Figure S6 (Supporting Information).

[Mo$_2$(9H-3,6-CDC)$_2$(DMPU)]$_6$·xS, 3A. Following the same procedure as that for **1A**, a 1:2 molar ratio of $Mo_2(O_2CCF_3)_4$ (16 mg, 0.025 mmol) and H_2(9H-3,6-CDC) (13 mg, 0.050 mmol) reacted in 1.7 mL of DMPU with 1 drop of HBF$_4$ (40% in water) at 85 °C for 2 days. Single crystals were collected, washed with DMPU, and quickly dried to afford 10 mg of [Mo$_2$(9H-3,6-CDC)$_2$(DMPU)]$_6$·xS (**3A**). FT-IR (neat, cm^{-1}): 2937(w), 2861(w), 1702(w), 1601(s), 1521(s), 1448(m), 1382(s), 1316(m), 1250(m), 1216(m), 1125(w), 1105(w), 1057(m), 1023(w), 939(w), 772(w), 752(m), 709(m), 670(m). This product is unstable in air and insoluble in water, MeOH, and EtOH but slightly soluble in DMF, DEF, and DMSO. The PXRD pattern of as-synthesized **3A** is shown in Figure S7 (Supporting Information).

[Mo$_2$(4,4′-CDDB)$_2$(S)$_{7/6}$]$_6$·xS, 3B. Following the same procedure as that for **1A**, a 1:2 molar ratio of $Mo_2(O_2CCF_3)_4$ (16 mg, 0.025 mmol) and H_2(4,4′-CDDB) (20 mg, 0.050 mmol) reacted in 1.7 mL of DMA with 1 drop of HBF$_4$ (40% in water) at 100 °C for 6 days. Single crystals were collected, washed with DMA, and quickly dried to afford 9 mg of [Mo$_2$(4,4′-CDDB)$_2$(S)$_{7/3}$]$_6$·xS (**3B**). FT-IR (neat, cm^{-1}): 2923(w), 2876(w), 1653(s), 1598(w), 1496(m), 1456(m), 1391(s), 1301(m), 1260(m), 1190(m), 1112(w), 1026(w), 984(w), 925(w), 902(w), 855(w), 815(w), 775(m), 744(w), 705(m). This product is unstable in air and insoluble in water, MeOH, EtOH, DMF, DEF, and DMSO. The PXRD pattern of as-synthesized **3B** is shown in Figure S8 (Supporting Information).

[Mo$_2$(1,3-BDC)$_2$(DMPU)(S)$_{2/3}$]$_{12}$·(DMPU)$_8$·xS, 4A. Following the same procedure as that for **1A** but without the addition of HBF$_4$, a 1:2 molar ratio of $Mo_2(OAc)_4$ (11 mg, 0.025 mmol) and H_2(1,3-

BDC) (8 mg, 0.050 mmol) reacted in 1.5 mL of DMPU at 110 °C for 4 days. Single crystals were collected, washed with DMPU, and quickly dried to afford 8 mg of $[Mo_2(1,3\text{-BDC})_2(DMPU)(S)_{2/3}]_{12}\cdot(DMPU)_8\cdot xS$ (**4A**). FT-IR (neat, cm^{-1}): 3440(w), 2931(w), 2862(w), 1704(w), 1605(s), 1558(w), 1514(s), 1472(w), 1438(m), 1406(w), 1378(m), 1317(m), 1272(w), 1254(m), 1215(m), 1130(w), 1106(w), 1058(m), 936(w), 886(w), 835(w), 754(m), 738(m), 724(s), 708(m), 664(m). This product is unstable in air and insoluble in water, MeOH, EtOH, DMF, DEF, and DMSO. The PXRD pattern of as-synthesized **4A** is shown in Figure S9 (Supporting Information).

$[Mo_2(5\text{-OH-1,3-BDC})_2(DMPU)(S)]_{12}\cdot(DMPU)_8\cdot xS$, 4B. Following the same procedure as that for **1A** but without the addition of HBF$_4$, a 1:3 molar ratio of $Mo_2(O_2CCF_3)_4$ (16 mg, 0.025 mmol) and $H_2(5\text{-OH-1,3-BDC})$ (14 mg, 0.075 mmol) reacted in 1.5 mL of DMPU at 85 °C for 12 days. Single crystals were collected, washed with DMPU, and quickly dried to afford 4 mg of $[Mo_2(5\text{-OH-1,3-BDC})_2(DMPU)(S)]_{12}\cdot(DMPU)_8\cdot xS$ (**4B**). FT-IR (neat, cm^{-1}): 2930(w), 2867(w), 1587(s), 1538(w), 1518(s), 1445(w), 1399(m), 1372(w), 1318(m), 1274(w), 1251(w), 1214(m), 1122(w), 1103(w), 1056(m), 1018(w), 976(w), 940(w), 890(w), 808(w), 764(m), 729(s), 676(m). This product is unstable in air and insoluble in water and EtOH but slightly soluble in DMF, DEF, and DMSO. The PXRD pattern of as-synthesized **4B** is shown in Figure S10 (Supporting Information).

$[Mo_2(5\text{-}t\text{-Bu-1,3-BDC})_2(S)_{11/6}]_{12}\cdot xS$, 4C. Following the same procedure as that for **1A** but without the addition of HBF$_4$, a 1:2 molar ratio of $Mo_2(O_2CCF_3)_4$ (16 mg, 0.025 mmol) and $H_2(5\text{-}t\text{-Bu-1,3-BDC})$ (11 mg, 0.050 mmol) reacted in 1.5 mL of DMA at 100 °C for 6 days. Single crystals were collected, washed with DMA, and quickly dried to afford 10 mg of $[Mo_2(5\text{-}t\text{-Bu-1,3-BDC})_2(S)_{11/6}]_{12}\cdot xS$ (**4C**). FT-IR (neat, cm^{-1}): 2938(w), 1617(s), 1518(s), 1437(w), 1399(m), 1357(s), 1314(w), 1265(m), 1187(m), 1113(w), 1058(w), 1012(m), 960(w), 908(w), 824(w), 763(m), 728(s), 695(w). This product is unstable in air and insoluble in water, MeOH, EtOH but slightly soluble in DMF, DEF, and DMSO. The PXRD pattern of as-synthesized **4C** is shown in Figure S11 (Supporting Information).

$[Mo_2(2,7\text{-NDC})_2(S)_2]_{12}\cdot xS$, 4D. Following the same procedure as that for **1A** but without the addition of HBF$_4$, a 1:2 molar ratio of $Mo_2(O_2CCH_3)_4$ (11 mg, 0.025 mmol) and $H_2(2,7\text{-NDC})$ (11 mg, 0.050 mmol) reacted in 1.7 mL of DMF at 85 °C for 10 days. Single crystals were separated from brown precipitate by repeatedly washing with DMF (precipitate can be suspended in the solvent, but crystals sink rapidly) and then quickly dried to afford 4 mg of $[Mo_2(2,7\text{-NDC})_2(S)_2]_{12}\cdot xS$ (**4D**). FT-IR (neat, cm^{-1}): 2923(w), 1643(s), 1501(m), 1427(w), 1385(s), 1355(s), 1254(w), 1236(w), 1194(w), 1145(w), 1097(m), 1058(w), 959(w), 928(w), 855(w), 824(w), 802(w), 782(m), 755(w), 697(w). This product is unstable in air and insoluble in water, MeOH, EtOH, DMF, DEF, and DMSO. The PXRD pattern of as-synthesized **4D** is shown in Figure S12 (Supporting Information).

Single-Crystal X-ray Diffraction Study. Data were collected on a Bruker SMART APEX-II diffractometer with a low-temperature device and a fine-focus sealed-tube X-ray source (Mo Kα radiation, $\lambda = 0.71073$ Å). A suitable single crystal was picked up directly from the mother liquor with a Nylon loop glued to a pin and quickly transferred to a cold stream of liquid nitrogen (110 K) for data collections. Raw data collection and reduction were manipulated using APEX2 software.[23] The semiempirical method SADABS[24] was applied for absorption corrections. The structures were solved by direct methods and refined by the full-matrix least-squares technique against F^2 with the anisotropic temperature parameters for all non-hydrogen atoms using the SHELXTL software package.[25] All hydrogen atoms were geometrically placed

(23) *APEX2 software package*, Bruker Molecular Analysis Research Tool, v. 2008.4; Bruker AXS Inc.: Madison, WI, 2008.
(24) Sheldrick, G. M. *SADABS*, Program for Absorption Correction of Area Detector Frames; Bruker AXS Inc.: Madison, WI.
(25) Sheldrick, G. M. *Acta Crystallogr., Sect. A* **2008**, *64*, 112–122.

Table 3. Crystal Data and Structure Refinement of **3A** and **3B**

	3A	3B
formula	$C_{204}H_{156}Mo_{12}N_{24}O_{54}$	$C_{312}H_{180}Mo_{12}N_{12}O_{55}$
formula weight	4958.81	6127.96
crystal system	hexagonal	triclinic
space group	$R\bar{3}$	$P\bar{1}$
crystal size, mm	0.30 × 0.28 × 0.26	0.22 × 0.18 × 0.18
a, Å	34.997(3)	28.410(11)
b, Å	34.997(3)	28.674(11)
c, Å	39.893(7)	45.274(17)
α, deg	90	91.126(5)
β, deg	90	91.473(6)
γ, deg	120	105.233(6)
V, Å^3	42 315(9)	35 560(23)
Z	3	2
$d_{calc,}$ g cm^{-3}	0.584	0.572
reflections collected	147 966	261 869
(before SQUEEZE)	(160 794)	(261 900)
independent reflections	18 472 [$R_{int} = 0.0840$]	87 865 [$R_{int} = 0.1938$]
(before SQUEEZE)	(20 806 [$R_{int} = 0.1213$])	(87 875 [$R_{int} = 0.3321$])
data/restraints/parameters	18 472/44/344	87 865/9/1234
(before SQUEEZE)	(20 806/44/344)	(87 875/8/1348)
GOF	1.004	0.683
R_1, wR_2^{a}	0.0618, 0.1402	0.0632, 0.1225
(before SQUEEZE)	(0.1291, 0.4572)	(0.2084, 0.5684)

^{a} The value of R_1 is based on "observed" data with $I > 2\sigma(I)$; the value of wR_2 is based on all data.

and refined in riding model approximation. There are large pore volumes in the crystal structures of some compounds, which are occupied by heavily disordered solvent molecules. In some cases, the positions of solvent molecules can be found, and a satisfactory disorder model can be achieved. However, this cannot be done for all solvent molecules; therefore, the SQUEEZE program implemented in PLATON was used to model this electron density.[26] The program calculated a solvent-accessible volume, which was then removed from subsequent structure factor calculations. The structures were refined further using the data generated. In some cases, for the coordinated solvents only O atoms were left and refined. The contents of the solvent region are not represented in the unit cell contents in crystal data. Attempts to determine the final formula of such compounds from the SQUEEZE results combined with elemental analysis (EA) were unsuccessful because of the volatility of the crystallization solvents during EA measurements; therefore, accurate data set cannot be obtained. Tables 1–4 list crystal data and refinement results for all compounds. Additional structure refinement details (most of them are included in CIFs) can be found in the Supporting Information.

Gas Adsorption Measurement. Before adsorption, about 120 mg of an as-synthesized sample of **4C** was soaked in deoxygenated distilled methanol under a nitrogen atmosphere for 24 h, and the extract was discarded. Fresh methanol was subsequently added, and the sample was allowed to stay in methanol for an additional 24 h before methanol was removed. This procedure was repeated twice. After the methanol extract was decanted, the sample was dried under a dynamic vacuum (<10^{-3} Torr) at room temperature for 5 h. Before adsorption measurement, the sample was further activated using the "outgas" function of the adsorption analyzer for 5 h at 50 °C. Finally, 98 mg of a brown amorphous sample was used in the gas adsorption measurement. High-purity grade N$_2$ and O$_2$ gases were used in the adsorption experiments.

Results and Discussion

Design, Synthesis, and Characterization. Twelve rigid dicarboxylate linkers have been designed to explore the effects of bridging angle, ligand size, and ligand substituent on the formation of metal–organic architectures based on square four-connected Mo–Mo nodes. In these ligands, two carboxylate

(26) Spek, A. L. *J. Appl. Crystallogr.* **2003**, *36*, 7–13.

Table 4. Crystal Data and Structure Refinement of **4A**−**4D**

	4A	4B	4C	4D
formula	$C_{312}H_{336}Mo_{24}N_{40}O_{124}$	$C_{312}H_{336}Mo_{24}N_{40}O_{152}$	$C_{288}H_{288}Mo_{24}O_{118}$	$C_{288}H_{144}Mo_{24}O_{120}$
formula weight	8932.77	9380.77	7939.74	7826.59
crystal system	monoclinic	tetragonal	triclinic	hexagonal
space group	$P2_1/n$	$I4/m$	$P\bar{1}$	$P6_3/m$
crystal size, mm	$0.22 \times 0.20 \times 0.20$	$0.20 \times 0.18 \times 0.16$	$0.40 \times 0.20 \times 0.20$	$0.18 \times 0.16 \times 0.16$
a, Å	26.83(3)	31.651(8)	25.6486(16)	33.052(2)
b, Å	33.23(3)	31.651(8)	25.682(3)	33.052(2)
c, Å	27.88(3)	32.246(16)	29.181(3)	33.833(4)
α, deg	90	90	65.4810(10)	90
β, deg	91.117(14)	90	63.9820(10)	90
γ, deg	90	90	86.8650(10)	120
V, Å^3	24 857(44)	32 305(20)	15 524(2)	32 009(5)
Z	2	2	1	2
d_{calc}, g cm^{-3}	1.193	0.964	0.849	0.812
reflections collected	199 735	87 022	119 919	308 668
(before SQUEEZE)	(199 838)	(89 134)	(123 708)	(310 319)
independent reflections	35 889 [R_{int} = 0.2945]	16 056 [R_{int} = 0.1430]	54 325 [R_{int} = 0.0688]	19 068 [R_{int} = 0.1639]
(before SQUEEZE)	(35 905 [R_{int} = 0.4634])	(16 681 [R_{int} = 0.1874])	(56 657 [R_{int} = 0.0794])	(19 359 [R_{int} = 0.2522])
data/restraints/parameters	35 889/224/1105	16 056/46/527	54 325/226/1618	19 068/296/491
(before SQUEEZE)	(35 905/224/1105)	(16 681/46/526)	(56 657/226/1619)	(19 359/296/492)
GOF	0.804	1.012	1.027	1.018
R_1, wR_2^{a}	0.0812, 0.1893	0.0754, 0.1805	0.0618, 0.1404	0.0768, 0.1660
(before SQUEEZE)	(0.1451, 0.4350)	(0.1359, 0.4211)	(0.1437, 0.4481)	(0.1452, 0.4614)

^{a} The value of R_1 is based on "observed" data with $I > 2\sigma(I)$; the value of wR_2 is based on all data.

groups acting as coordination donors are separated by organic entities, which have geometrically fixed angles based on their inherent configurations. Thus, each ligand acts as an angular linker when two carboxylate groups coordinate to two nodes simultaneously. The angular bridging of these linkers and the planar four-connected propagation of Mo−Mo nodes can lead to the formation of either discrete molecular architectures or two-dimensional layers, but only discrete molecules were harvested in this work. The bridging angle and size of a ligand control the shape and size of the resulting assembly, whereas the non-coordination substituent affects only its property. Furthermore, several ligands were newly synthesized for this systematic study, adding new members to the multitopic carboxylate ligand library useful in the construction of other metal−organic architectures.

In the synthesis of these Mo−Mo cluster-based compounds, the starting material containing a quadruply bonded Mo−Mo unit was $Mo_2(O_2CCF_3)_4$ or $Mo_2(OAc)_4$. It is well-known that the CF_3COO^- or OAc^- group can be easily replaced by another carboxylate. Attempts to use other Mo sources, such as $Mo(CO)_6$ and $MoCl_3$, to synthesize these compounds were unsuccessful. The ligand-substitution reaction was carried out under solvo-thermal conditions in a sealed and oxygen-free container. The products were harvested as single crystals in each case. The addition of an inorganic acid (here, HBF_4) in some cases presumably helps lower the reaction rate, thereby giving good crystalline products. In all compounds except **1A**, trapped free solvent molecules easily escape when crystals leave the mother liquor, leading to a loss of crystallinity. Thus, these crystals are unstable, and the larger the assembly, the less stable it becomes. In addition, all of the products are moderately oxidation-sensitive in the solid state and are easily oxidized when wet or in solution. Both crystal instability and oxidation sensitivity of these compounds add difficulty to the determination of their composition, especially the content of guest solvent molecules. However, the structure determination from single-crystal X-ray diffraction together with the purity evaluation from powder X-ray diffraction of bulk samples (see the Supporting Information) have provided evidence for the molecular structures and synthetic reliability of these complex molecular assemblies.

Table 5. Mo−Mo Bond Distances in the Molecular Metal−Organic Assemblies Reported in This Work

	$d_{\text{Mo−Mo}}$ (Å)
1A	2.102(3)
1B	2.1144(7)
1C	2.1059(12)
2A	2.115(2)−2.120(2)
2B	2.108(1)−2.118(1)
2B′	2.110(2)
2C	2.105(2)
3A	2.1041(5)
3B	2.093(1)−2.116(1)
4A	2.116(2)−2.145(3)
4B	2.108(1)−2.113(1)
4C	2.1090(7)−2.1160(8)
4D	2.1295(9)−2.135(1)

Assembly and Crystal Structures. Structures of all resulting molecular metal−organic architectures have been determined by single-crystal X-ray diffraction analyses. Molecular structures are shown in Figures 3−6, and Mo−Mo bond distances are listed in Table 5. These bond distances are typical for Mo−Mo quadruple bonds, confirming the Mo_2^{4+} oxidation state in the final products,[27] consistent with the spectroscopic studies in solution (*vide infra*).

Lantern-Type 1A−1C. With their "parallel" arrangement of the two carboxylate groups in a ligand, 3,3′-(pyridine-2,6-diyl)dibenzoate (3,3′-PDDB^{2-}), 3,3′-[1,3-phenylenebis(ethyne-2,1-diyl)]dibenzoate (3,3′-PBEDDB^{2-}), and 3,3′-(2-amino-5-isopropyl-1,3-phenylene)bis(ethyne-2,1-diyl)dibenzoate (2-NH$_2$-5-*i*-Pr-3,3′-PBEDDB^{2-}) anions can be viewed as having a bridging angle of 0°. Their assembly with Mo−Mo dimer gave three isostructural compounds, [Mo$_2$(3,3′-PDDB)$_2$(S)]$_2$ (**1A**), [Mo$_2$(3,3′-PBEDDB)$_2$(NMP)$_2$]$_2$ (**1B**), and [Mo$_2$(2-NH$_2$-5-*i*-Pr-

(27) Cotton, F. A. Molybdenum compounds. In *Multiple Bonds between Metal Atoms*, 3rd ed.; Cotton, F. A., Walton, R. A., Murillo, C. A. Eds.; Springer Science + Business Media: New York, 2005.
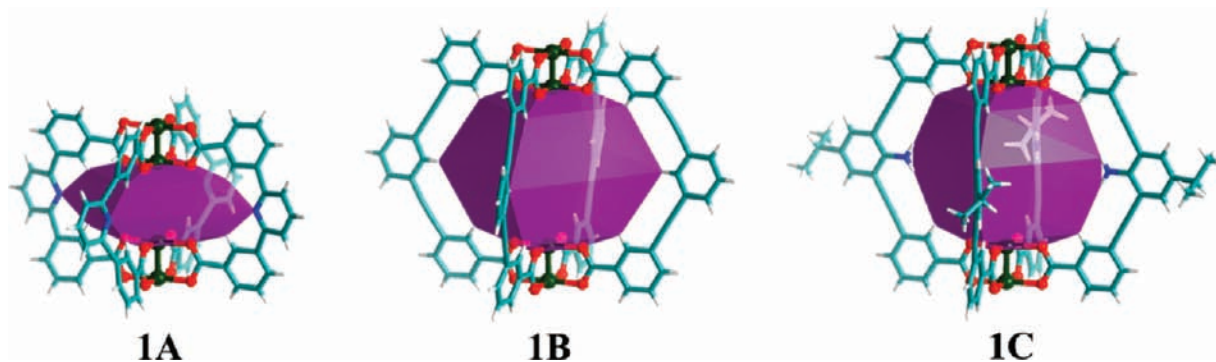
Figure 3. Molecular structures of **1A**, **1B**, and **1C**. The purple polygon represents the void inside each cage. Mo, dark green; O, red; C, teal; N, blue; H, white; all solvent molecules including those coordinated to Mo−Mo units are omitted for clarity.
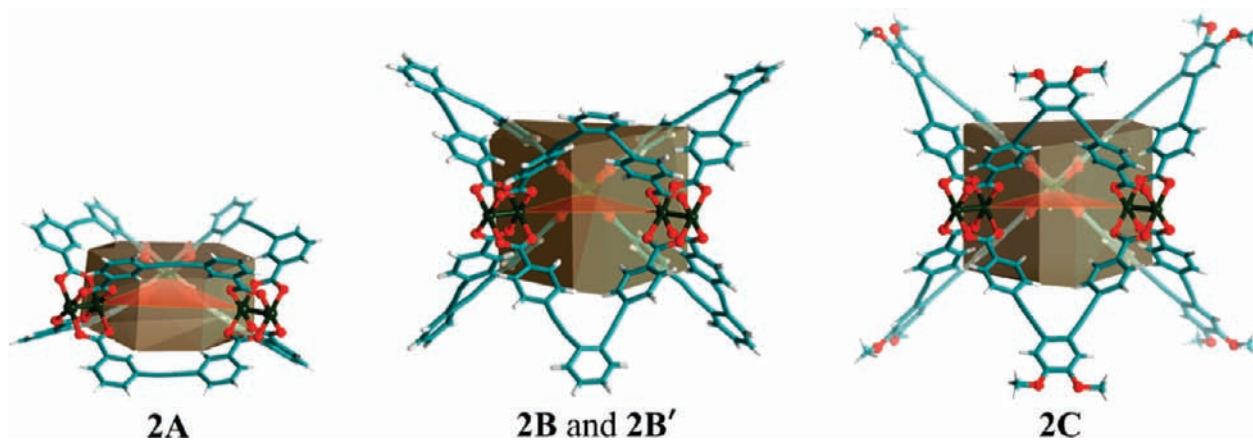
Figure 4. Molecular structures of **2A**, **2B/2B′**, and **2C**. The dark gray prism within each molecular ring represents the size of the largest prism that would occupy the cavity. The red trigonal plane represents the Mo−Mo clusters' arrangement in the molecule. Mo, dark green; O, red; C, dark cyan; H, white; all solvent molecules including those coordinated to Mo−Mo units are omitted for clarity.

3,3′-PBEDDB)$_2$(DMSO)$_2$]$_2$·(DMSO)$_4$ (**1C**). These molecular cages have a lantern-type structural arrangement with four bridging ligands surrounding two Mo−Mo units to form a large "paddlewheel" (Figure 3). The arrangement of the two Mo−Mo dimers in these structures is linear, in contrast to those polygons and polyhedra in other structures described below. The molecular dimensions of the three cages excluding coordinated solvents in height (Mo···Mo) and diameter (H···H between two opposite ligands) are 9.0 × 20.0, 14.0 × 23.0, and 14.0 × 27.0 Å, respectively, and the internal cavities are 5.0 × 13.0, 10.0 × 14.0, and 10.0 × 11.0 Å (atom-to-atom distances across opposite Mo and H atoms of ligands). Although the first two ligands with 0° bridging angle are different in size, they gave rise to the same lantern-type structure. It is also evident that the size of the cage can be tuned simply by varying the length of the two arms of a ligand. In addition, from the structures of **1B** and **1C**, one can conclude that, when the bridging angle of a ligand is fixed, the additional functionalization of the ligand does not have an effect on the topological structure of the resulting assembly. It should be pointed out that, during the preparation of this manuscript, a Cu$_2$-based compound of ligand 3,3′-PBEDDB^{2-} with a structure similar to that of **1B** was reported, which was described as an edge-directed tetragonal metal−organic polyhedron.[11k] In addition, a few compounds

with structural topology similar to that of **1A**−**1C** have also been reported, although those compounds were constructed from pyridine-based bridging ligands and square planar Pd(II) nodes.[10b,28]

Trigonal 2A−2C. The *cis* configuration of ligand 3,3′-(ethyne-1,2-diyl)dibenzoate (3,3′-EDDB^{2-}) anion has a 60° bridging angle. Its assembly with the Mo−Mo dimeric unit led to a molecular "ring" with six linkers bridging three Mo−Mo units in a trigonal prismatic way, [Mo$_2$(3,3′-EDDB)$_2$(S)$_2$]$_3$·xS (**2A**, Figure 4). The approximate size of the molecular ring is 20.0 Å in diameter and 10.0 Å in height. If the Mo−Mo units are viewed as vertices, this molecule forms an equilateral triangle with an edge length of 11.3 Å. The geometrical topology of this molecule is similar to that of a reported paddlewheel Cu$_2$-based chiral compound of a half-rigid ligand, *N,N′*-terephthaloyl-bis(L-phenylalaninato).[11f] The assembly of the other ligand in Figure 2 having a 60° bridging angle, 4,4′-(1,2-phenylene)bis(ethyne-2,1-diyl)dibenzoate (4,4′-PBEDDB^{2-}), with the Mo−Mo dimer also gave a ring molecule, [Mo$_2$(4,4′-PBEDDB)$_2$(X)]$_3$·xS [**2B**, X = $^5/_3$DMA + $^1/_3$S, and **2B′**, X = 2S, crystallized in different space groups due to the different molecular packing in the crystals], as shown in Figure 4. The structure of **2B** is also similar to that of a reported compound assembled by an angular bridging pyridine-based ligand and square coordinated Pd(II) ion.[29] The height and diameter of the molecular ring are 17.0 and 22.0 Å, and the edge length of the Mo−Mo equilateral

(28) (a) McMorran, D. A.; Steel, P. J. *Angew. Chem., Int. Ed.* **1998**, *37*, 3295−3297. (b) Yue, N.; Qin, Z.; Jennings, M. C.; Eisler, D. J.; Puddephatt, R. J. *Inorg. Chem. Commun.* **2003**, *6*, 1269−1271. (c) Chand, D. K.; Biradha, K.; Fujita, M. *Chem. Commun.* **2001**, 1652−1653.

(29) Suzuki, K.; Kawano, M.; Fujita, M. *Angew. Chem., Int. Ed.* **2007**, *46*, 2819−2822.
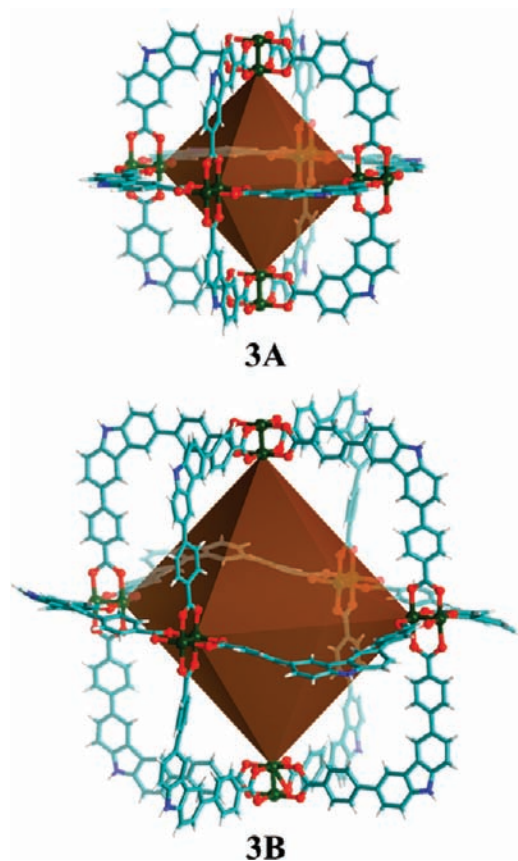
Figure 5. Molecular structures of **3A** and **3B**. The brown polyhedron within each molecular cage represents the polyhedral presentation of the molecular cage when considering Mo–Mo clusters as vertices and ligands as edges. Mo, dark green; O, red; C, dark cyan; N, blue; H, white; all solvent molecules including those coordinated to Mo–Mo units are omitted for clarity.

triangle is 11.0 Å. Again, despite the different lengths of the carboxylate arms and distinct shapes of the two ligands, the formation of the molecular ring can be solely ascribed to the 60° bridging angle. The height and diameter of the ring can be tuned by ligand modification that preserves the bridging angle. Functionalizing 4,4′-PBEDDB^{2-} with two methoxy groups results in the new ligand 4,4′-(4,5-dimethoxy-1,2-phenylene)bis-(ethyne-2,1-diyl)dibenzoate (4,5-(MeO)$_2$-4,4′-PBEDDB^{2-}). This ligand assembled with Mo–Mo units to give the compound [Mo$_2$(4,5-(MeO)$_2$-4,4′-PBEDDB)$_2$(S)$_2$]$_3$·xS (**2C**), having a structural topology similar to that of **2B**. Again, functionalization of the ligand does not affect the geometrical structure of the resulting assembly.

Octahedral 3A and 3B. Two carbazole-based dicarboxylate ligands, 9H-3,6-carbazoledicarboxylate (9H-3,6-CDC^{2-}) and 4,4′-(9H-carbazole-3,6-diyl)dibenzoate (4,4′-CDDB^{2-}), with a nearly 90° bridging angle assembled with a Mo–Mo dimer to give two isostructural polyhedral cages, [Mo$_2$(9H-3,6-CDC)$_2$(DMPU)]$_6$·xS (**3A**) and [Mo$_2$(4,4′-CDDB)$_2$(S)$_{7/6}$]$_6$·xS (**3B**). As shown in Figure 5, both molecular cages have an octahedral arrangement of the Mo–Mo units, reminiscent of a Cu$_2$-based counterpart with 9H-3,6-CDC^{2-} ligand reported earlier from this laboratory.[11j] The cage size of **3A** is 25.0 Å in diameter when viewed as a sphere, and the internal cavity size is 15.0 Å across. The average edge length of a triangular window in the cage is 10.5 Å. The cage size, internal cavity size, and open window size for **3B** are 38.0, 23.0, and 17.0 Å, respec-

tively. Evidently, the bridging angle controls the geometric shape of the cage, and the size of the molecular architecture is tuned by varying the ligand size.

Cuboctahedral 4A, 4B, 4C, and 4C′ and Anti-cuboctahedral 4A′ and 4D. When a Mo–Mo dimer assembled with each of the four bridging ligands having a 120° bridging angle, 1,3-benzenedicarboxylate (1,3-BDC^{2-}), 5-hydroxy-1,3-benzenedicarboxylate (5-OH-1,3-BDC^{2-}), 5-*tert*-butyl-1,3-benzenedicarboxylate (5-*t*-Bu-1,3-BDC^{2-}), and 2,7-naphthalenedicarboxylate (2,7-NDC^{2-}), much more complicated cage compounds were obtained: [Mo$_2$(1,3-BDC)$_2$(X)]$_{12}$·xS [**4A**, X = DMPU + $^2/_3$S, and **4A′**, X = xS,[15] having the same composition of metal and bridging ligands but different structures], [Mo$_2$(5-OH-1,3-BDC)$_2$(DMPU)(S)]$_{12}$·(DMPU)$_8$·xS (**4B**), [Mo$_2$(5-*t*-Bu-1,3-BDC)$_2$(X)]$_{12}$·xS [**4C**, X = $^{11}/_6$S, and **4C′**, X = pyridine,[15] with different coordinated terminal solvent molecules on Mo–Mo clusters], and [Mo$_2$(2,7-NDC)$_2$(S)$_2$]$_{12}$·xS (**4D**). The four compounds **4A**, **4B**, **4C**, and **4C′** are isostructural, with differences only in nonbridging functional groups on the ligands and/or axially coordinated solvents (Figure 6). If bridging linkers are viewed as linear edges and Mo–Mo units as vertices, these molecules have a cuboctahedral metal clusters arrangement, similar to that for their Cu$_2$-based counterparts.[11a–c,15]

It is evident that, no matter how large or different in shape the ligands are, what nonbridging functional group(s) is on a ligand, and which metal (Mo or Cu) provides the square connecting node, the geometric shape of the molecular assembly is almost always dominated by the bridging angle of the rigid linker.

However, bridging angle alone cannot explain the following stereoisomerization of cuboctahedron and anti-cuboctahedron. Unlike **4A**, **4B**, **4C**, and **4C′**, molecular cages **4A′** and **4D** have an anti-cuboctahedral arrangement of their Mo–Mo units (Figure 6). When viewed as a sphere, molecular cage **4D** has a diameter of 31.0 Å. Its internal cavity size is 22.0 Å. The open windows of the molecular cage are quadrangular and triangular in shape and 11.0 Å in edge length for both types of openings. Molecular cage **4A′**, which was synthesized by a reaction between Mo$_2$(OAc)$_4$ and H$_2$(1,3-BDC) in DMF in the presence of pyridine, is isostructural with **4D** but a stereoisomer of **4A**. The structural difference between **4A** and **4A′** arises from the subtle variation in arrangements of the two triangular cupolas of the anti-cuboctahedron (also known as triangular bicupola) and cuboctahedron, as elucidated in a previous report from this laboratory.[15] The mechanism that accounts for this isomerization is difficult to study because the two molecular cages are almost identical sterically and energetically.

In addition, the Mo–Mo units in all the molecular architectures are often axially coordinated by solvent molecules, especially when the solvent, such as NMP and DMPU, is a good terminal ligand. If one changes the terminal ligand to a bridging ditopic linker, the molecular architectures can be extended into MOFs.

Supramolecular Assembly of 2B′. Another interesting feature is the supramolecular assembly observed in the crystal structure of **2B′**. As shown in Figure 7, in the crystal structure four **2B′** molecules are assembled to form a new supramolecular cage. The four molecules arrange in a tetrahedral fashion, with each occupying one vertical position. The resulting supramolecular cage has an internal cavity of about 20.0 Å in diameter and four triangular intermolecular-formed windows. This supramolecular cage is surrounded and further reinforced by four additional **2B′** molecules in the four
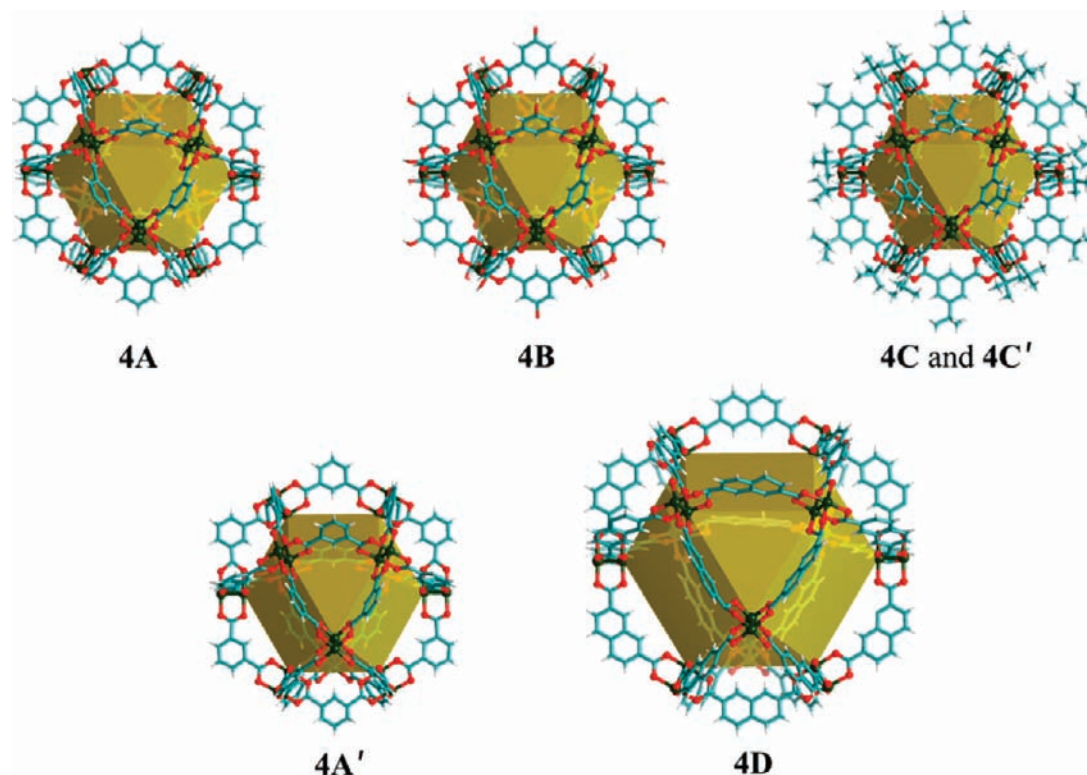
Figure 6. Molecular structures of **4A**, **4A′**, **4B**, **4C/4C′**, and **4D**.[15] The green-yellow polyhedron within each molecular cage represents the polyhedral presentation of the molecular cage when considering Mo–Mo clusters as vertices and ligands as edges. Mo, dark green; O, red; C, dark cyan; H, white; all solvent molecules including those coordinated on Mo–Mo units are omitted for clarity.

window positions by virtue of π--π interactions between ligand benzene groups to form a more complex supramolecular capsule. These assemblies thus result in the crystallization of **2B′** in the highly symmetric cubic space group $P\bar{4}3n$. Although many supramolecular entities assembled by weak interactions have been reported, such a fascinating structure from the packing of metal–organic molecular architectures acting as building units is unprecedented, reflecting the "subtleness" of supramolecular assembly and the balance of the weak interactions.[30]

Spectroscopic and Electrochemical Properties of Selected Members. It has also been demonstrated that the introduction of a nonbridging functional group (isopropyl, imino/amino, methoxyl, hydroxyl, or *tert*-butyl) into a linker changes the solubility of the resulting molecular architecture, albeit the bridging angle and size of an organic linker determine the geometric shape and size of the resulting molecular architecture, respectively. For example, **1C**, **2C**, **3A**, **4B**, and **4C** are slightly soluble in DMF, DEF, and DMSO. This allows us to study the spectroscopic and electrochemical properties of these dimolybdenum-based compounds in solution. The absorption spectra of **1C**, **3A**, **4B**, and **4C** in DMF or DMSO are shown in Figure 8. The absorption maxima located in the range of 442–468 nm can be ascribed to the $\delta \rightarrow \delta^*$ transition.[31] The cyclic voltammogram of **4B** was measured in DMF with tetrabutylammonium hexafluorophosphate as supporting electrolyte (Figure 9). The redox pair with half-wave potential of 0.9 V corresponds to

Mo_2^{4+}/Mo_2^{5+} of an isolated Mo–Mo unit with little or no communication among adjacent Mo–Mo pairs.

Gas Adsorption of 4C. In order to evaluate the porosity of these Mo–Mo cluster-based molecular materials, at least on those polyhedral cages, as a representative example N_2 and O_2 adsorption measurements of guest-evacuated **4C** was carried out at 77 K. Before adsorption measurements, the sample **4C** was vacuum-dried at room temperature and at 50 °C after solvent exchange in order to obtain the guest-free cage. As shown in Figure 10, N_2 sorption of guest-free **4C** gave a type-I adsorption isotherm, implying that this material possesses permanent porosity. The apparent monolayer surface area and pore volume of guest-free **4C** were estimated from the N_2 adsorption data to be 504 m^2 g^{-1} (437 m^2 g^{-1} for BET model) and 0.20 cm^3 g^{-1}, respectively. An uptake capacity of 130 cm^3 g^{-1} was reached at 77 K and near 1 atm. A whole hysteresis of desorption was observed in the isotherm, which probably is attributed to the adsorption of the space between molecular cages which are formed through molecular packing in solid state. Additionally, the activation of **4C** might lead to a packing structure having the window of the cage partially blocked by adjacent cages, inhibiting gas molecular diffusion during desorption. Indeed, after guest-removal, the sample became amorphous. This may be attributed to the position rearrangement of the molecular cages of **4C** with respect to one another upon activation.[5,11d,g] However, at the molecular level, the individual cage structure of **4C**, and thus its porosity, should be maintained, as demonstrated by the N_2 adsorption.

O_2 adsorption at 77 K follows a behavior similar to that of N_2 with a slight hysteresis of desorption (Figure 10). O_2 uptake of 188 cm^3 g^{-1} was reached at 77 K and 154 mmHg. It should

(30) Steed, J. W.; Atwood, J. L. *Supramolecular Chemistry*, 2nd ed.; John Wiley & Sons Ltd.: Chichester, UK, 2009.

(31) Cotton, F. A. Physical, spectroscopic and theoretical results. In *Multiple Bonds between Metal Atoms*, 3rd ed.; Cotton, F. A., Walton, R. A., Murillo, C. A. Eds.; Springer Science + Business Media:New York, 2005.
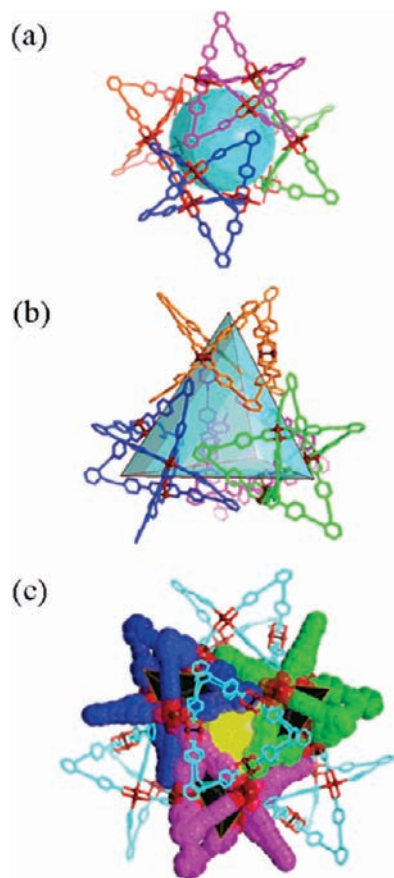
Figure 7. Supramolecular assembly of **2B′** in the crystal structure, highlighting the resulting cage (a), tetrahedral array of **2B′** molecules (b), and final capsule (c).
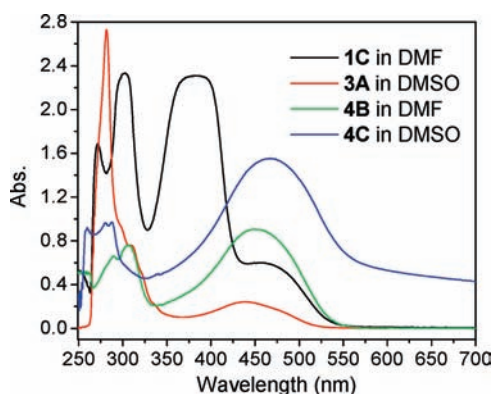

**Figure 8.** Absorption spectra of **1C**, **3A**, **4B**, and **4C**.

be pointed out that, after O_2 adsorption, a subsequent N_2 adsorption measurement on the same sample showed no uptake (Figure 10), implying the collapse of the molecular cage, presumably combined with the oxidization of Mo^{4+} clusters by remaining O_2.[32] Further investigations are needed to figure out the reason behind this loss of gas adsorption ability, and related works are in progress in this laboratory.

Conclusions

A systematic exploration of bridging-angle-driven assembly of molecular architectures which contain quadruply bonded

(32) Cotton, F. A.; Murillo, C. A.; Zhou, H.-C. *Inorg. Chem.* **2000**, *39*, 3261–3264.
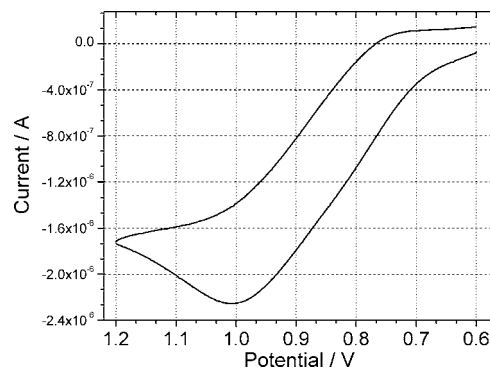
Figure 9. CV spectrum of **4B** in DMF.
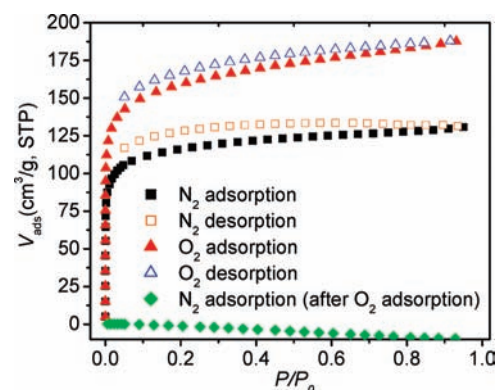
Figure 10. N_2 and O_2 adsorption/desorption isotherms of guest-free **4C** at 77 K. P and P_0 are the equilibrium and saturation pressure, respectively (designed at $P_0 = 757$ for N_2 and 154 mmHg for O_2 at 77 K).

Mo–Mo units has been performed by using 12 dicarboxylate ligands with four different bridging angles. The results have shown that the shape and size of the resulting molecular architecture can be controlled by tuning the bridging angle and size of the linker, respectively. Functionalization of the linker can adjust the solubility of the ensuing molecular assembly but has little or no effect on the geometry of the product. Primary spectral and electrochemical properties have also been explored on selected members. Furthermore, gas adsorption experiments confirmed the porosity of these molecular cages in the solid state, at least at the molecular level. The synthesis and structural control/tuning of the Mo–Mo cluster-based molecular assembles reported here is a crucial first step for the further exploration of their properties and functions. Eventually, we also hope these studies will lead to a general synthetic strategy for the preparation of MOFs containing metal–metal bonds using the molecular metal–organic assemblies as precursors or molecular building units.

Supporting Information Available: Schemes (and detailed procedures in some cases) for the synthesis of new ligands, additional details for structure refinement, crystallographic information files (CIFs), and PXRD patterns (simulated and experimental) for **1A–4D**. This material is available free of charge via the Internet at http://pubs.acs.org.